MATERIALS CHEMISTRY
FRONTIERS

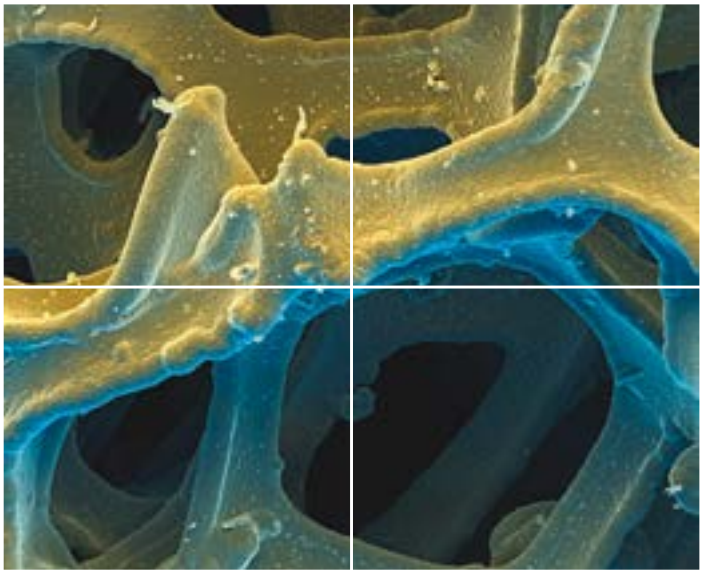

Accepted Manuscript

This article can be cited before page numbers have been issued, to do this please use: Z. Kang, S. Wang, R. Wang, H. Guo, B. Xu, S. Feng, L. Fan, L. Zhu, W. Kang, J. Pang, H. Sun, X. Du, M. Zhang and D. Sun, *Mater. Chem. Front.*, 2018, DOI: 10.1039/C8QM00351C.

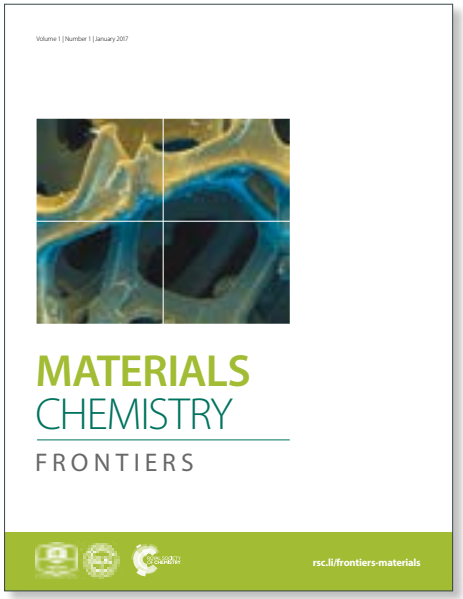

This is an Accepted Manuscript, which has been through the Royal Society of Chemistry peer review process and has been accepted for publication.

Accepted Manuscripts are published online shortly after acceptance, before technical editing, formatting and proof reading. Using this free service, authors can make their results available to the community, in citable form, before we publish the edited article. We will replace this Accepted Manuscript with the edited and formatted Advance Article as soon as it is available.

You can find more information about Accepted Manuscripts in the author guidelines.

Please note that technical editing may introduce minor changes to the text and/or graphics, which may alter content. The journal's standard Terms & Conditions and the ethical guidelines, outlined in our author and reviewer resource centre, still apply. In no event shall the Royal Society of Chemistry be held responsible for any errors or omissions in this Accepted Manuscript or any consequences arising from the use of any information it contains.

View Article Online
DOI: 10.1039/C8QM00351C

Journal Name

ARTICLE

Sandwich Membranes through a Two-dimensional Confinement Strategy for Gas Separation

LiuReceived 00th January 20xx,
Accepted 00th January 20xx

DOI: 10.1039/x0xx00000x

www.rsc.org/

Zixi Kang,†[a] Sasa Wang,†[a] Rongming Wang,[a] Hailing Guo,[b] Ben Xu,[a] Shou Feng,[a] Lili Fan,[a] Liangkui Zhu,[c] Wenpei Kang,[a] Jia Pang,[a] Hanyi Sun,[a] Xinxin Du,[a] Minghui Zhang,[a] Daofeng Sun*[a]

Metal-organic frameworks (MOFs) with designable pore environment can be involved into graphene oxide (GO) layers as the filters to tailor the channels in laminar membranes for precisely molecular separation. The well-distributed fillers, high compatibility between fillers and GO, and thin selective layers are critical aspects to capitalize on the positive effect induced by the addition of microporous phase. Here, a two-dimensional confinement strategy to constructing the composite membrane is deduced by *in situ* conversing the metal hydroxide/GO precursors to MOF/GO "sandwich" membranes. This method is confirmed to be feasible for the creation of an ultra-thin composite membrane with uniformly MOF fillers dispersion in and well compatibility with GO layers. The sandwich membranes show enhanced H_2/CO_2 separation performance: H_2 permeance of 5922±1000 GPU and H_2/CO_2 selectiviy of 75±4 at 25 °C, which is six-fold increased compared with the GO membrane. Due to the combination of GO and MOF, the membrane also exhibited a H_2 permeance of 3654 ± 252 GPU and a H_2/CO_2 selectivity of 31 ± 3 at 150 °C with the feed gas containing water vapor. Such a nanoscale confinement approach can be extended to other composite membranes, providing valuable insights in designing and developing of advanced materials for membrane-based efficient molecular separation.

Introduction

Ultra-thin membranes with uniform pore size are promising candidates for efficient separation process.[1-6] Graphene oxide (GO), as a type of two-dimensional material, can be engineered into ultra-thin membranes for molecular separation through the in-plane defects and the spacing between GO layers.[7-10] However, the channels in GO membranes are of variable sizes and difficult to be tailored for selective permeation of light gases and monovalent ions.[7] Several pioneering studies have been reported to adjust the interlayer spacing by cationic controlling,[10] varying humidity,[11] crosslinking and inserting other species, etc.[12-16] Even so, significant efforts are still demanded to be devoted to develop uniform, high-density, subnanosized pores in GO membranes for efficient sieving of light gases or small ions.[9, 10, 17] Similar to doping porous materials into polymers to prepare mixed matrix membranes (MMMs),[18-24] metal-organic frameworks (MOFs), a kind of microporous and designable materials with uniform pore sizes,[25-30] can be intercalated into the gaps of GO layers as microporous fillers to sieve mixtures.[31, 32] Recently, Yao et al. reported a UiO-66-NH_2/GO membrane, which exhibited enhanced hydrogen separation performance with an H_2/N_2 and H_2/CO_2 ideal selectivity of 9.75 and 6.35, respectively.[33] Zhang and Liu et al. prepared an antimicrobial ZIF-8/GO thin film nanocomposite membranes for nanofiltration.[34] Zhong and Liu et al. reported MOF@GO membranes prepared by pressure-assisted self-assembly filtration technique for pervaporation.[35] Wang et al. studied vacuum-assisted assembly of ZIF-8@GO composite membranes with enhanced organic solvent nanofiltration performance.[36] There are some key points to produce MOFs/GO composite membranes for efficient molecular separation: (i) interfacial adhesion between the MOFs and GO layers; (ii) homogeneous dispersion of MOFs in the GO membrane; (iii) thin selective layers to give ideal permeance. Suitable strategies are required to fulfill these requirements based on the layered structure of the GO and crystal growth process of MOFs.

Inspired by the filler nanosizing and *in situ* coordination strategies in the polymer MMMs system,[19, 22, 37-40] two-dimensional confinement conversion method was performed in this work to fabricate MOF/GO sandwich membranes by *in situ* reacting of hydroxides nanosheets (NS)/GO precursor membranes and organic ligands.[41, 42] As illustrated in **Scheme 1**, metal hydroxides NS were evenly amalgamated with GO sheets and the metal hydroxides/GO membranes were fabricated via a vacuum filtration process. Subsequently, the

[a] College of Science, China University of Petroleum (East China), Qingdao, Shandong 266580, PR China, E-mail: dfsun@upc.edu.cn.
[b] State Key Laboratory of Heavy Oil Processing, Key Laboratory of Catalysis, China National Petroleum Corp. (CNPC), China University of Petroleum (East China), Qingdao 266555, PR China.
[c] State Key Laboratory of Inorganic Synthesis and Preparative Chemistry, Jilin University, Changchun 130012, P. R. China.
† These authors contribute equally to this work.
Electronic Supplementary Information (ESI) available: [details of any supplementary information available should be included here]. See DOI: 10.1039/x0xx00000x

View Article Online
DOI: 10.1039/C8QM00351C

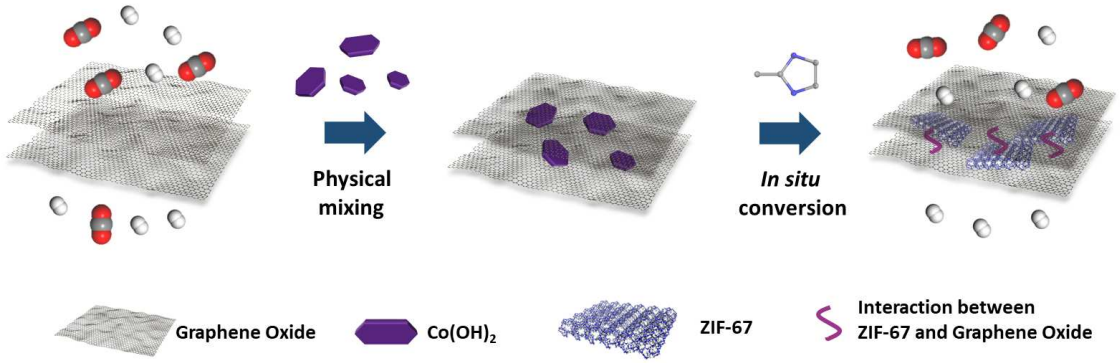

Scheme 1 Schematic illustration of sandwich membranes through the two-dimensional confinement strategy for gas separation.

metal hydroxides NS incorporated play the role of metal source, which in situ assemble with organic linker through the formation of coordination bonds. It is worth mentioning that the MOF fillers are generated in the layered GO matrix, thus resulting in their well combination. Moreover, owing to the two-dimensional confinement effect of GO layers, the obtained membranes can maintain the uniform distribution of fillers and ultra-thin thickness.[43] Through *in situ* temperature-dependent FTIR spectroscopy, it was found that CO_2 molecules were sealed in the membrane, and we suggest that it is associated with the hydrogen bonds formed between CO_2 and GO as well as CO_2 and ZIF-67. The strong interaction between CO2 and the membrane further hinders the CO_2 passage. Mixed gas permeance tests of the MOF/GO sandwich membranes were performed, and the results showed a highly enhanced selectivity level for H_2/CO_2 separation. We are pleased to demonstrate that this two-dimensional confinement conversion strategy works well and should be generally applicable for other microporous materials/graphene oxide systems, such as *in situ* crystallization of dry-gel precursor to zeolite in lamellar GO membranes.[44, 45]

Experimental

Materials

The Nylon membrane filters (pore size 0.2 μm, diameter 47 mm) were obtained from GE. Graphene oxide (GO) was provided by XFNANO. $Co(Ac)_2{\cdot}4H_2O$, 2-methylimidazole (2-MIM, 98%) were provided by Energy Chemical. Ammonia solution and hydrazine hydrate (85%) were supplied by Sinopharm Chemical Reagent Co., Ltd. All the chemical materials were used as received.

Synthesis of $Co(OH)_2$ NS

0.6225 g $Co(Ac)_2{\cdot}4H_2O$ was dissolved into 200 mL DI water, then 175 μL hydrazine hydrate (85%) and 5 mL ammonia solution were added into the solution, which was kept at 95 °C under backflow for 1.5 h. After self-cooling, the $Co(OH)_2$ suspension was centrifuged and washed thoroughly with DI water for several times, and then dried at 80 °C.

Preparation of $Co(OH)_2$/GO-x and ZIF-67/GO-x membranes

0.05 g GO was dispersed in 500 mL DI water by sonication for 1 h to obtain the GO suspension (0.1 g L^{-1}). 0.01 g $Co(OH)_2$ NS was dispersed into 75 mL DI water by sonication for 0.5 h. 25 mL GO suspension was added into the suspension above by sonication for 0.5 h to form a $Co(OH)_2$/GO suspension. The $Co(OH)_2$/GO-x membranes (x was the volume of $Co(OH)_2$ NS/GO suspension in mL) with different thickness were obtained by filtration of different volume of $Co(OH)_2$/GO suspension (20 mL, 25 mL, 30 mL, 35 mL, 40 mL) onto the Nylon substrates. 50 mL 2-MIM solution (20 g L^{-1}) was filtered on the $Co(OH)_2$/GO-x membranes for 48 h to converse $Co(OH)_2$ to ZIF-67. When the color of the membrane was changed to purple, the ZIF-67/GO-x membranes were obtained.

Preparation of ZIF-67/GO-D membranes

1.52 mg nano-sized ZIF-67 crystals (referred to ZIF-67 NC) was dispersed into 75 mL DI water by sonication for 0.5 h. 25 mL GO suspension (0.1 gL^{-1}) was added into the suspension above and by sonication for 0.5 h. 20mL, 30mL, 40mL dispersions were filtered onto Nylon support to obtain ZIF-67/GO-D membranes.

Characterization

The morphologies of all materials and membranes were observed with a scanning electron microscope (SEM, HITACHI, S4800). TEM images were performed with a JEM-2100 (JEOL Co. Japan) at the accelerating voltage of 200 kV. Atomic force microscope (AFM) instrument (Bruker) was used to investigate the microcosmic structure of the prepared materials. In order to obtain AFM images, samples were dripped and dried on the Si wafer and imaged on a commercial Multi Mode Scanning Probe Microscope with a NanoScope IVa controller in contact mode. For the membrane samples, the composite membranes were scraped from the Nylon supports, dispersed in the ethanol via sonication. After second order flattening, all height images were directly analyzed using NanoScope Analysis software an Ultima X-ray diffractometer to observe the structure information. X-ray photoelectron spectroscopy (XPS) (version 1.40, Bruker) to obtain section profiles along the fibril axis. Powder X-ray diffraction (PXRD) tests were carried out on results were collected with a Kratos AXIS Ultra DLD surface analysis instrument. BET surface area of the samples was

View Article Online
DOI: 10.1039/C8QM00351C

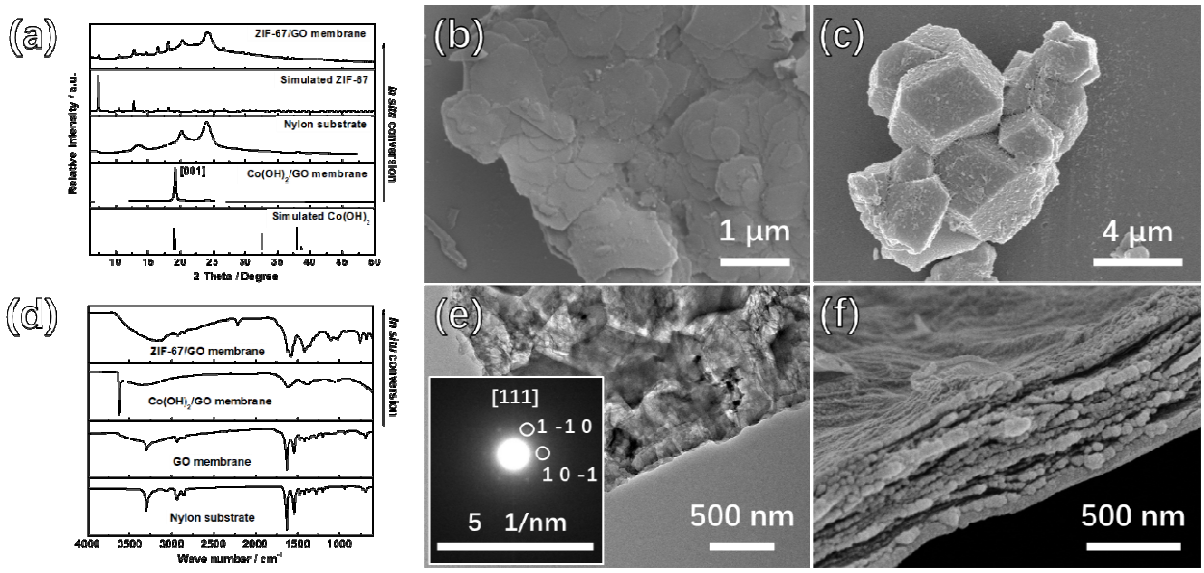

Fig. 1 *In situ* conversion from $Co(OH)_2$/GO to ZIF-67/GO sandwich membranes. (a, d) PXRD and FTIR spectra for the membranes before and after *the* conversion process. (b) SEM image of $Co(OH)_2$ NS. (c) SEM image of the ZIF-67 conversed from $Co(OH)_2$ NS without GO. (e) TEM and (f) cross-section SEM images of ZIF-67/GO membrane.

calculated from the N_2 adsorption-desorption isothermal curve at 77K. The powder samples were tested with Micro ASAP2020 to analyze the gas adsorption-desorption performance of H_2 (99.995%) and CO_2 (99.995%) at both 273 K and 298 K. For the experimental set-up of gas-separation measurement, themembrane was set in a stainless steel cell at room temperature and standard atmospheric pressure. One side of the membrane was swept by argon, while the other side was exposed to single gases or gas mixtures. A soap-film flow meter was used to measure the gas flux of Argon and feed gases before the test. The membrane would be fixed by two O-rings in the cell. To prevent damage to membrane surface caused by the contact with O-rings, the edge of the membrane was covered by foil-tape, leaving a 10-mm-diameter circular membrane surface. The mixed feed flow rates were constant with a total volumetric flow rate of 100 mL/min (50 mL/min of each gas, 1:1 mixture), controlled by mass flow controllers (MFCs). Argon was used as a sweep gas to minimize the influence of back diffusion of the sweeping gas to the feed side. The sweep gas flow rate was 80 mL/min to eliminate concentration polarization in the permeate side. There was no pressure drop between the sides of the membranes, in order to prevent any distortion of the membrane.[5, 46, 47] The calibration curves were made by the fitting of more than eight points each. The value of each point was based on more than twenty GC parallel tests. The permeate flow rate of test gases was calculated from the corresponding GC results and calibration curves. (SHIMADZU GC-2014C). The permeability, termed permeance (P_i, GPU, 1 GPU = 3.3928×10^{-10} $mol\cdot m^{-2}\cdot s^{-1}\cdot Pa^{-1}$), of the MOFs membrane, was calculated with the following Equation 1:

$$P_i = N_i / (\Delta p_i \times A) \quad (1)$$

where N_i ($mol\cdot s^{-1}$) is the permeate flow rate of component i, Δp_i (Pa) is the trans-membrane pressure drop of i, and A (m^2) is the membrane area.

The membrane permselectivity was evaluated by the selectiviy ($\alpha_{i,j}$), which was obtained according to Equation 2:

$$\alpha_{i,j} = P_i / P_j \quad (2)$$

where i, j represent the two components in the permeate mixture, respectively.

Results and discussion

Preparation and Characterization of Sandwich Membrane

The ZIF-67/GO sandwich membranes were prepared as a proof of the concept. ZIF-67 is a classical MOF with a uniform pore size (3.4 Å) and stable structure, which is suitable for gas separation.[48] The Co sources, amalgamation approaches, and the ratio of ZIF-67 precursor/GO have important influences on the successful preparation of the sandwich membrane. Several attempts have been carried out to fabricate the suitable precursor membranes, and the preparation conditions for different membranes were summarized in **Table S1**.

Co_3O_4 NS were firstly selected as the precursor of ZIF-67, which were unfavorable for ZIF-67 conversion since the slow release rate of cobalt ion (**Fig. S1a**). Therefore, in order to increase the release rate, $Co(OH)_2$ NS was chosen as the precursor because that it is amphoteric hydroxide that can effectively release cobalt ions in 2-MIM solution. The mixing approaches of *in situ* growth of $Co(OH)_2$ on the GO was firstly applied to expect a well combination, however irreversible agglomeration of GO resulted in the destruction of the layered structure of the membrane (**Fig. S1b**). Thus, $Co(OH)_2$ NS were separately synthesized and physically mixed with GO

View Article Online
DOI: 10.1039/C8QM00351C

dispersions. The SEM, TEM, and AFM images (**Fig. 1b and Fig. S1c-d**) were collected to demonstrate the morphology of $Co(OH)_2$ NS. We can learn that the diameter of $Co(OH)_2$ NS is in the range of 0.5~2.5 μm, and the thickness is around 4 nm. As revealed in the selected-area electron diffraction (SAED, inset of **Fig. S1d**) and PXRD (**Fig. 1a**), the pure phase of $Co(OH)_2$ was obtained. The very strong diffraction peak at 19.1^o corresponds to the (0 0 1) crystal plane of $Co(OH)_2$, which further demonstrates the directional growth of the $Co(OH)_2$ NS.

The $Co(OH)_2$/GO precursor membranes were prepared by vacuum filtration of different volumes of $Co(OH)_2$/GO suspension onto the Nylon substrates. And the optimized ratio of $Co(OH)_2$: GO was demonstrated to be 4: 1 (**Table S1**). Varied volumes of $Co(OH)_2$/GO suspension (20 mL, 25 mL, 30 mL, 35 mL, and 40 mL) were applied to obtain the $Co(OH)_2$/GO-x (x denotes the consumed volume of the $Co(OH)_2$/GO suspension) membranes with different thickness. The top-view and cross-section SEM images, as shown in **Fig. S2-3**, indicated the continuous surfaces and ultra-thin thickness of the membranes. The XRD results further demonstrate that $Co(OH)_2$ was successfully filled between GO since the clear $Co(OH)_2$ peaks for all membranes. (**Fig. S4**).

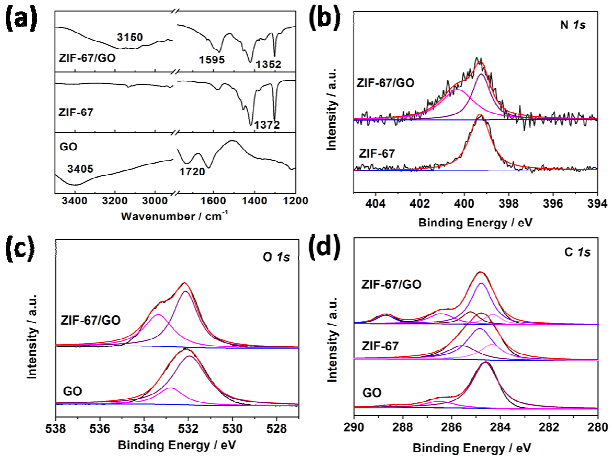

Fig. 2 (a) FTIR spectra of GO, ZIF-67, and ZIF-67/GO. (b)N 1s, (c) O 1s, and (d) C 1s XPS spectra for GO, ZIF-67, and ZIF-67/GO.

The 2-MIM solution was added to the surface of membranes to conduct conversion process before the precursor membranes were completely dry, forming adhesion between membranes and Nylon substrates during the *in situ* transformation process. The conversion process was carried out at room temperature for 48 hours to obtain the final membranes. During the *in situ* transformation process, membranes were adhered to the Nylon substrates and were difficult to scrape from the substrates, suggesting a robust membrane product. The color of the 2-MIM solution changed to purple after the *in situ* conversion process, implying the release of Co^{2+} ions of from $Co(OH)_2$ and self-assembly of ZIF-67 from dissolved Co^{2+} and 2-MIM.

No $Co(OH)_2$ peaks present in the PXRD pattern and the peaks of ZIF-67 are observed, as shown in **Fig. 1a** and **Fig. S5a,** indicating the successful conversion from $Co(OH)_2$ NS to ZIF-67. Furthermore, as shown in the inset of **Fig. 1e**, the interplanar spacing of the (1 -1 0) planes calculated from the SAED patterns was ~1.163 nm, which is in agreement with the value obtained from the XRD pattern of ZIF-67, indicating the forming of MOF. However, the PXRD pattern for ZIF-67/GO-20 membrane prepared with the least precursor presents invisible peaks of ZIF-67, which may be attributed to the low content of MOFs. To prove this point, we prepared the membrane by direct mixing the ZIF-67 crystals and GO with the same ZIF-67/GO ratio of ZIF-67/GO-20 membrane. The PXRD pattern of this membrane was shown in **Fig. S5b**, and there was no obvious peak of ZIF-67 in the pattern. The conversion from $Co(OH)_2$ to ZIF-67 can be further confirmed by the FTIR measurements (**Fig. 1d**, **Fig. 2a,** and **Fig. S6**). After the transformation, the peaks at 750 and 1400 cm^{-1} appeared, attributed respectively to the out of plane vibration and stretching vibration of the imidazole ring related to ZIF-67 became evident. More importantly, the peaks at 1720 cm^{-1} for C=O stretching vibration and 3405 cm^{-1} for O-H stretching vibration from GO shift to lower frequency at 1630 cm^{-1} and 3150 cm^{-1} respectively for ZIF-67/GO.[49] While the peak for C-N stretching vibrations shifts from 1376 cm^{-1} to 1353 cm^{-1}, compared to that of pure ZIF-67. These are assigned to the formation of hydrogen bond between different groups on GO and the ZIF-67.[50]

The XPS tests were carried out to study chemistry between GO and MOF as well (**Fig. 2b-d**). The N 1s spectrum of ZIF-67/GO-40 membrane can be deconvoluted into two peaks, -C-N- (399.2 eV) that present in pure ZIF-67 and a new peak at 400.3 eV. The peak at 400.3 eV is assigned to nitrogen atoms from 2-MIM bonded to the GO layer via the hydrogen bond,[51] which was consistent with the FTIR results. On the other hand, O 1s component peaks shift from 531.9 eV (C=O) and 532.8 eV (O-C=O, C-O-C) to 532.1 eV and 533.4 eV respectively. These results showed an increased electron cloud density of C atoms while a decreased electron cloud density of O atoms, suggesting that the 2-MIM in ZIF-67 could form hydrogen bonds with the O atoms of GO.[52, 53] The bonding strength can

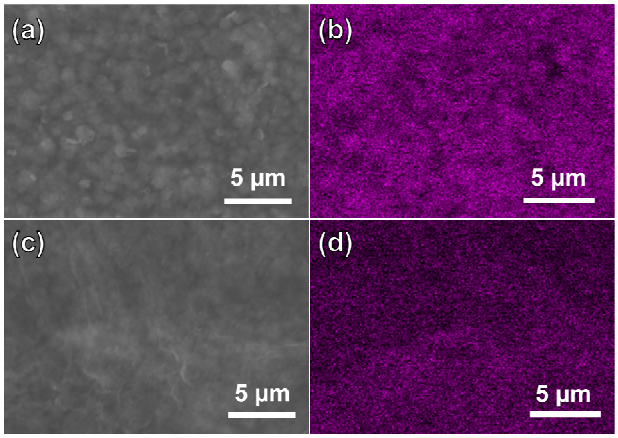

Fig. 3 Top-view SEM and Co EDS mapping of (a, b) $Co(OH)_2$/GO-40 and (c, d) ZIF-67/GO-40 membrane.

View Article Online
DOI: 10.1039/C8QM00351C

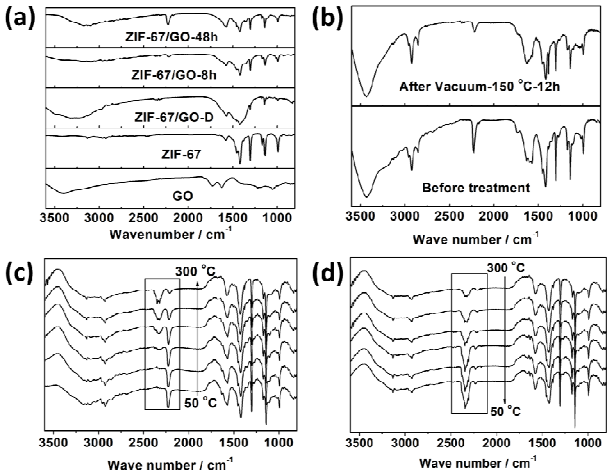

Fig. 4 (a, b) Comparison of *off situ* FTIR spectrogram for different samples. (c, d) *in situ* temperature dependent FTIR results of sample scraped from ZIF-67/GO membrane.

prevent the interfacial micro-gaps and reduce the possibility of selectivity loss. In addition, the C1s peaks of ZIF-67/GO membranes were deconvoluted into -C-OH (286.5 eV), -C=C-/-C-C- (284.3 eV) and -C=O (288.7 eV) that from GO, -C=N (285.3 eV), -C-N (284.8 eV) originally in ZIF-67 (**Fig. 2d** and **Table S2**). The enhanced intensity of C=O (288.7 eV) was caused by the sealed CO_2 in the membranes, which would be discussed below.

To check the actual loading amounts of ZIF-67 in conversed membranes, the inductive coupled plasma emission spectrometer (ICP) characterization was carried out on the different membranes. The membranes were heated to ~500°c in the air then dissolved in acid to perform the ICP tests, and the results were summarized in **Table S3**. The ratios of ZIF-67/GO increased with the volume of filtration solution, while all the values were less than the initial mixing ratios. These results further confirmed the fact that during the transformation process, part of the cobalt source was conversed to ZIF-67, while the other part was dissolved in the 2-MIM solution. ICP tests were also carried out on the reaction solution after the conversion for ZIF-67 /GO-20 and ZIF-67/GO-40, and the results were shown in **Table S4**. Based on the coordination equilibrium, higher metal ions concentration in the 2-MIM solution of ZIF-67/GO-40 made the equilibrium shift in the ZIF-67 formation direction, which resulted in the higher ZIF-67 ratio in the membranes.

Expectedly, the continuously and laminar ZIF-67/GO membrane structure was achieved employing this *in situ* conversion strategy, thanks to the two-dimensional confinement effect served by GO layers. If the conversion process was carried out without GO, ZIF-67 crystals with the size of 3-4 μm were obtained (**Fig. 1c**). For the ZIF-67/GO membranes with a varied thickness of around 130, 250, 330, 400, and 500 nm, corresponding to ZIF-67/GO-20, 25, 30, 35 and 40, respectively, can be examined from the cross-section SEM images (**Fig. S7** and **S8**). It is obvious that the layered membranes were not burst open by conversed ZIF-67 (**Fig. S9**), which implies the small thickness of ZIF-67. Furthermore, as revealed by the EDS mapping of precursor and conversed membrane (**Fig. 3**), the cobalt element dispersed uniformly in the GO matrix, suggesting that ZIF-67 was evenly formed from $Co(OH)_2$ precursor in the composite membranes. The AFM images, shown in **Fig. S10**, further illustrates that the thickness of the samples scraped from the ZIF-67/GO membranes were below 20 nm.

To further study the two-dimensional confinement effect of GO layers during the conversion process, the $Co(OH)_2$ powders and $Co(OH)_2$/GO membranes after different conversion time (2h, 8h, 16h, 36h, and 48h) were monitored by PXRD and SEM, and the results were summarized in **Fig. S11** and **S12**. For the pure $Co(OH)_2$ precursor, ZIF-67 crystals with the size of around 1 μm began to form on the surfaces of the precursors after 8 hours, as confirmed by the SEM image. After 36 hours, all $Co(OH)_2$ transformed to ZIF-67 crystals, which corresponds to the PXRD and FTIR results. Eventually, the ZIF-67 crystals reached 3-4 μm after 48 hours (**Fig. S12j**). In contrast to the pure $Co(OH)_2$ precursor, the XRD peaks corresponding to ZIF-67 cannot be noticed in the $Co(OH)_2$/GO membranes until 36 hours after the conversion began, and the wide peaks suggest the nanosized feature of conversed ZIF-67. The SEM images of the converted membranes (**Fig. S12a-e**) present no microcrystalline of ZIF-67 on their tops, and the ZIF-67/GO membranes presented continuous and relatively smooth surfaces. The ZIF-67/GO-D membranes were prepared by directly mixing Nano-sized ZIF-67 (referred to ZIF-67 NC) and GO for comparison. The loading amounts of ZIF-67 NC in ZIF-67/GO-D-20, 30 and 40 membranes were controlled according to the ratio in respective of ZIF-67/GO-x membranes. As revealed in **Fig. S13**, the size of ZIF-67 NC was around 400 nm, the composite membranes are not smooth, and the large size of ZIF-67 NC caused many defects in the membranes. These results suggest that the two-dimensional confinement of GO layers played a key role in maintaining the laminar morphology of the membranes.

There is one noticeable phenomenon from the ATR-FTIR results. It is interesting that a new peak at 2225 cm^{-1}, ascribed to neither GO nor ZIF-67, appeared during the conversion process (**Fig. 1d** and **4a**). Although this strong peak is quite similar to the nitrile peak, it is less possible that the C≡N bond can be formed at this moderate condition. Therefore, the *in situ* temperature-dependent FTIR measurements were performed on the membrane samples to better understand this peak. A self-made *in situ* sample stage and temperature controlling system were employed for the *in situ* temperature-dependent FTIR measurements, and the results were shown in **Fig. 4c** and **4d**. It is obvious that the 2225 cm^{-1} peak almost remain unchanged below 150 °C, although the slight drop in its intensity and small red-shift are detected, which can be ascribed to the heating effects. However, the intensity drastically drops above 150 °C, meantime, the wide band related to free CO_2 simultaneously grows. For further illustrating the originates of this peak, the FTIR spectra of ZIF-67/GO membranes before and after annealing treatment in

View Article Online
DOI: 10.1039/C8QM00351C

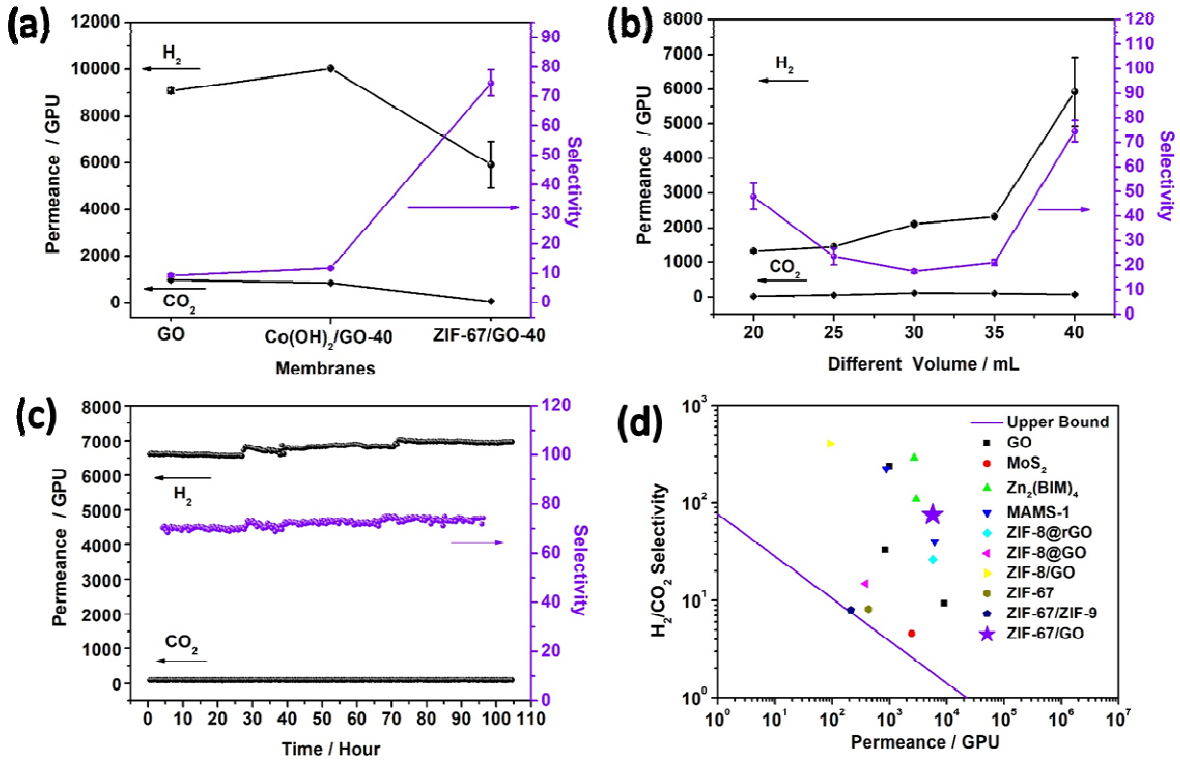

Fig. 5 (a) H_2/CO_2 mixed gases separation performances on GO membrane, $Co(OH)_2$/GO-40 MMMs and ZIF-67/GO-40 composite membranes. (b) H_2/CO_2 mixed gases separation performances on the ZIF-67/GO composite membranes with different thickness at 25°C. (c) The plot of H_2/CO_2 permeance and selectivity for the ZIF-67/GO-40 composite membrane versus test time. (d) H_2/CO_2 selectivity as a function of H_2 permeability for ZIF-67/GO-40 membrane compared with other 2D and ZIF-67 structure based membranes reported in the literature [54], 13, [55], 1, 5, 32, [56], [57] and [58] (**Table S6**). The upper bound lines of H_2/CO_2 for polymer membranes are plotted according to reference[59], assuming a membrane thickness of 200 nm.

the vacuum oven at 150 °C for 12 hours were collected (**Fig. 4b**). The strong 2225 cm^{-1} peak evidently weakens after annealing treatment, and the CO_2 peak at 2340 cm^{-1} is not observed.[60, 61] Therefore, we can conclude that the 2225 cm^{-1} peak is ascribed to the CO_2 molecules fixed in the membrane through hydrogen bonding interactions between CO_2 and GO as well as CO_2 and ZIF-67.[62] The strong hydrogen bonding interactions shift the asymmetric stretch of CO_2 from 2340 cm^{-1} to 2225 cm^{-1}. In the ATR-FTIR results of the different membranes, it is clear that the sealed CO_2 peaks decrease with the membrane thickness, implying the CO_2 is sealed within the membrane rather than adsorbed at the surfaces (**Fig. S6b**).XPS results further support the existence of CO_2 due to the stronger peak at 288.4 eV and 533.4 eV (**Fig. 2d**). It is noteworthy that this new interaction can be ascribed to the synergistic effects between ZIF-67 and GO through the *in situ* conversion process, since neither ZIF-67, GO nor ZIF-67/GO physical mixtures perform such CO_2 peak in their FTIR spectra.

Gas sorption measurements of the fabricated membranes and pure GO were performed by physical gas adsorption. Calculated based on the N_2 adsorption isomers at 77 K (**Fig. S14a**), the BET surface area of ZIF-67/GO membranes was 540.8 $m^2 g^{-1}$, which was significantly increased compared with pristine GO (66.3 $m^2 g^{-1}$). These results could be attributed to the presence of ZIF-67 in the membrane that enhanced the free volume to facilitate the diffusion of gas molecules. The samples were evaluated on the H_2 and CO_2 adsorption property after BET tests. It is interesting that the H_2 and CO_2 adsorption amounts of ZIF-67/GO-40 decrease significantly compared with pure GO at 298 K (**Fig. S14b**). We examined the samples several times and had the same results. One possible reason is that the bond CO_2 prevents the gas being adsorbed within the membranes and the gas was only adsorbed to the surfaces.

Gas separation performance of the sandwich membrane

As discussed above, the advantages of homogeneous distribution of microporous fillers, suitable compatibility between fillers and matrix, and thin selective layers were achieved by in situ conversion process under two-dimensional confinement strategy, suggesting ZIF-67/GO membranes as a promising candidate for efficient light gases separation. The small window of ZIF-67 and the strong interaction between CO_2 and interlayers of sandwich membranes would imply the well hindering effects of the membrane on CO_2 passages, while

View Article Online
DOI: 10.1039/C8QM00351C

small H_2 molecules with weak affinity can easily pass through. Therefore, the sandwich membrane is expected to possess enhanced H_2/CO_2 separation performance compared with bare GO membranes.

Single gas permeation tests were carried out on the ZIF-67/GO membranes, and the results were summarized in **Fig. S15**. The low single gas permeation of CO_2 is due to the hybrid gas channels of ZIF-67/GO membrane, the strong diffusion resistance associated with the narrow window of the membrane and the adsorption effects. In the ZIF-67/GO composite membrane, both of the flexible interspaces of GO and the small ZIF-67 framework channels contribute to the hybrid gas permeation system. The strongly adsorbed CO_2 by ZIF-67, GO and their synergistic effect reduces its permeation rate in the single permeation tests. N_2 can permeate through the interlayer pores of GO but would be blocked by the ZIF-67 inserted. That is the reason N_2 possesses higher permeance than CO_2 but lower permeance than H_2.[63-65] Mixed gas (H_2/CO_2) separation studies were performed on the pure GO, $Co(OH)_2$/GO, and ZIF-67/GO-x membranes at 25°C (**Fig. 5a**). Compared with pure GO membrane, the H_2/CO_2 selectivity of ZIF-67/GO-40 sandwich membrane was increased by six-fold, from 9.3 ± 0.5 to 75 ± 4, and the permeance remained relatively high (H_2 = 5922± 1000 GPU). This separation performance was investigated from five different membranes (**Table S5**), proving the reproducibility of the membrane. The results demonstrated that the porous ZIF-67 fillers *in situ* assembled in the GO matrix were helpful in improving the gas separation performance.

The effects of the membrane thickness (or precursor solution volumes) on the separation properties were evaluated, and the separation performance for the membrane of each thickness was examined with two or more membranes and the same trend was obtained. As shown in **Fig. 5b**, the permeance of H_2 presented a rising trend with the increasing membrane thickness, while the H_2/CO_2 selectivity firstly decreased then increased. This phenomenon could be attributed to an integrated effect associated with the defects and thickness of the composite membranes. Involving ZIF-67 in GO expands the fractional free-volume (FFV) of the membrane and enhances gas permeance. However, it will also bring defects which are detrimental to the separation effects. Therefore, ZIF-67/GO-30 has the poorer H_2/CO_2 selectivity compared with its thinner counterparts, possibly due to the larger amounts of defects. Fortunately, the H_2/CO_2 selectivity recovered with continuous increasing of the thickness. However, the defects can be covered by more layers in the thicker membranes, contributing to better H_2/CO_2 selectivity performances in ZIF-67/GO-35 and ZIF-67/GO-40. We also attempted fabricating ZIF-67/GO-50 membrane to further evaluate the thickness effects; however, the membrane became too thick to stick to the Nylon support.

To study the temperature effect on gas permeance, mixed gas separation tests were carried out from 25°C to 150 °C on the ZIF-67/GO-40 membrane (**Fig. S16**). At higher temperature, a more activated CO_2 diffusion was resulted from the weakened adsorption of CO_2 by GO and ZIF-67, leading to a decrease of H_2/CO_2 selectivity. Similar phenomena have also been reported by other groups for 2D membranes.[46, 47, 66] The gas permeance increases substantially as the separation temperature increases, and the slightly decreased hydrogen permeability with temperature from 60 to 100 °C may be caused by the broken of hydrogen bonds between CO_2 and ZIF-67/GO membrane at high temperature, resulting in the larger amount of CO_2 that blocks the diffusion of H_2. The cycling performance of the ZIF-67/GO-40 membrane was evaluated by the continuous H_2/CO_2 permeance test up to 120 hours. No noticeable performance loss was detected (**Fig. 5c**), indicating its excellent stability for long-term continuous operations. The XRD and SEM characterizations were carried out on the ZIF-67/GO-40 membranes after a long time and high-temperature separation tests, and the results (**Fig. S17**) indicated that the structure and morphology of ZIF-67/GO-40 membranes were maintained well after a series of gas separation tests. As shown in **Fig. 5d** and **Table S6**, compared with other 2D membranes and ZIF-67 based membranes, the ZIF-67/GO sandwich membranes in this work showed a balance of permeance and selectivity and surpassed the 2008 upper bound line of polymer membranes. Therefore, the two-dimensional confinement strategy of involving MOFs fillers into GO was proved to be effective to improve gas separation performances.

For the practical appliation of pre-combustion CO_2 capture, the efficient H_2/CO_2 separation at real condtion (high temperature above 200 °C, feed gas with steam) is of the highest interest. Evaluating H_2/CO_2 separation performance at low temperature may guide the selection of promising candidates with high permeance and selectivity from the new materials. However, it is still challenging to apply the GO or MOF based membranes at the practical separation condition. For the GO based membranes, as hydration increases the GO spacing to ~ 0.9 nm,[8] and CO_2 shows higher solubility coefficient in water than any other gases.[67] The hydrothermal stability is one of the weakness for the MOF based polycrystalline membranes applied in the practical separation. Favorably, the ZIF-67/GO composite membrane can overcome the the cracks and inter-crystal defects of the polycrystalline membranes,[56] and the hierarchical structures or multiple transport mechanisms that may result in the water-facilitated CO_2 capture property.[68] To evaluate the separation performance at high temperature with water vapor, the ZIF-67/GO-40 membrane was heated to 150 °C (the Nylon substrates become brittle at 200 °C) and exposed to an equimolar H_2/CO_2 feed containing ~ 4 mol. % steam. The membrane exhibited a H_2 permeance of 3654 ± 252 GPU and a H_2/CO_2 selectivity of 31 ± 3, which is attractive values for the pre-combustion capture.[69] The significantly decreased gas permeance was due to the partial blockage of membrane pores,[70] and a more decreased CO_2 permeance was caused by the competitive sorption in the ZIF-67 micropores.[71] According to the competitive sorption theory, the presence of water vapor affects the permeation of high affinity components to a greater extent compared with the permeation of low affinity ones,[72] resulting in the increased selectivity compared with the membrane property tested at the dry condition. This separation performance at high temperature with steam

View Article Online
DOI: 10.1039/C8QM00351C

further indicates this ZIF-67/GO-40 membrane is a promising candidate for the practical application of pre-combustion CO_2 capture.

Conclusions

Laminar sandwich membranes of ZIF-67/GO were conversed from $Co(OH)_2$/GO precursors through a two-dimensional confinement strategy. The interaction between ZIF-67 and GO formed during the *in situ* conversion process. The ultra-thin membranes with evenly dispersed ZIF-67 showed a significantly enhanced gas separation performance of H_2/CO_2 mixture compared with the pristine GO membrane (H_2 Permeance of 5922 ± 1000 GPU and H_2/CO_2 selectivity of 75 ± 4) at 25 ^{o}C. Furthermore, the composite membrane can be stable at 150 ^{o}C with the feed gas containing steam, and possesses a H_2 permeance of 3654 ± 252 GPU and a H_2/CO_2 selectivity of 31 ± 3. Thanks to the diverse structures of MOFs and simple preparation process, the MOF/GO sandwich membrane prepared via the two-dimensional confinement strategy can be considered as potential materials for energy-efficient molecular separations. However, the understanding of mechanistic aspects of this conversion process to MOFs is still unclear. Some advanced operando characterization technology established in the nanoscience field can be readily applied to study the time-resolved dynamic issue in this system, which will be investigated in our future work.

Conflicts of interest

There are no conflicts to declare

Acknowledgements

This work was supported by National Natural Science Foundation of China (21501198, 21601205, 21771193, and 21571187), Taishan Scholar Foundation (ts201511019) and the Fundamental Research Funds for the Central Universities (18CX02047A, 18CX07001A).

Notes and references

1. Y. L. Yuan Peng, Yujie Ban, Hua Jin, Wenmei Jiao, Xinlei Liu, Weishen Yang, *Science*, 2014, **346**, 1356-1359.
2. M. Y. Jeon, D. Kim, P. Kumar, P. S. Lee, N. Rangnekar, P. Bai, M. Shete, B. Elyassi, H. S. Lee, K. Narasimharao, S. N. Basahel, S. Al-Thabaiti, W. Xu, H. J. Cho, E. O. Fetisov, R. Thyagarajan, R. F. DeJaco, W. Fan, K. A. Mkhoyan, J. I. Siepmann and M. Tsapatsis, *Nature*, 2017, **543**, 690-694.
3. W. J. Koros and C. Zhang, *Nat Mater*, 2017, **16**, 289-297.
4. H. B. Park, J. Kamcev, L. M. Robeson, M. Elimelech and B. D. Freeman, *Science*, 2017, **356**.
5. X. Wang, C. Chi, K. Zhang, Y. Qian, K. M. Gupta, Z. Kang, J. Jiang and D. Zhao, *Nat Commun*, 2017, **8**, 14460.
6. Y. Liu, Y. Ban and W. Yang, *Adv. Mater.*, 2017, **29**.
7. R. K. Joshi, P. Carbone, F. C. Wang, V. G. Kravets, Y. Su, I. V. Grigorieva, H. A. Wu, A. K. Geim and R. R. Nair, *Science*, 2014, **343**, 752-754.
8. B. Mi, *Science*, 2014, **343**, 740-742.
9. G. Liu, W. Jin and N. Xu, *Chem. Soc. Rev.*, 2015, **44**, 5016-5030.
10. L. Chen, G. Shi, J. Shen, B. Peng, B. Zhang, Y. Wang, F. Bian, J. Wang, D. Li, Z. Qian, G. Xu, G. Liu, J. Zeng, L. Zhang, Y. Yang, G. Zhou, M. Wu, W. Jin, J. Li and H. Fang, *Nature*, 2017, **550**, 380-383.
11. J. Abraham, K. S. Vasu, C. D. Williams, K. Gopinadhan, Y. Su, C. T. Cherian, J. Dix, E. Prestat, S. J. Haigh, I. V. Grigorieva, P. Carbone, A. K. Geim and R. R. Nair, *Nature nanotechnology*, 2017, **12**, 546–550.
12. M. Hu and B. Mi, *Environ. Sci. Technol.*, 2013, **47**, 3715-3723.
13. J. Shen, G. Liu, K. Huang, Z. Chu, W. Jin and N. Xu, *ACS nano*, 2016, **10**, 3398-3409.
14. K. Goh, W. Jiang, H. E. Karahan, S. Zhai, L. Wei, D. Yu, A. G. Fane, R. Wang and Y. Chen, *Adv. Funct. Mater.*, 2015, **25**, 7348-7359.
15. W.-S. Hung, C.-H. Tsou, M. De Guzman, Q.-F. An, Y.-L. Liu, Y.-M. Zhang, C.-C. Hu, K.-R. Lee and J.-Y. Lai, *Chem. Mater.*, 2014, **26**, 2983-2990.
16. H. Huang, Z. Song, N. Wei, L. Shi, Y. Mao, Y. Ying, L. Sun, Z. Xu and X. Peng, *Nat Commun*, 2013, **4**, 2979.
17. G. Liu, W. Jin and N. Xu, *Angew.Chem. Int. Ed.*, 2016, **55**, 13384 –13397.
18. P. Bernardo, E. Drioli and G. Golemme, *Ind. Eng. Chem. Res.*, 2009, **48**, 4638–4663.
19. J. Dechnik, J. Gascon, C. J. Doonan, C. Janiak and C. J. Sumby, *Angew. Chem. Int. Ed*, 2017, **56**, 2-21.
20. J. Dechnik, C. J. Sumby and C. Janiak, *Crystal Growth & Design*, 2017, DOI: 10.1021/acs.cgd.7b00595.
21. Z. Kang, Y. Peng, Z. Hu, Y. Qian, C. Chi, L. Y. Yeo, L. Tee and D. Zhao, *J. Mater. Chem. A*, 2015, **3**, 20801-20810.
22. Z. Hu, Z. Kang, Y. Qian, Y. Peng, X. Wang, C. Chi and D. Zhao, *Industrial & Engineering Chemistry Research*, 2016, **55**, 7933-7940.
23. T. Rodenas, M. van Dalen, E. García-Pérez, P. Serra-Crespo, B. Zornoza, F. Kapteijn and J. Gascon, *Adv. Funct. Mater.*, 2014, **24**, 249-256.
24. L. H. Wee, Y. Li, K. Zhang, P. Davit, S. Bordiga, J. Jiang, I. F. J. Vankelecom and J. A. Martens, *Adv. Funct. Mater.*, 2015, **25**, 516-525.
25. J. R. Li, R. J. Kuppler and H. C. Zhou, *Chem. Soc. Rev.*, 2009, **38**, 1477-1504.
26. H. Furukawa, K. E. Cordova, M. O'Keeffe and O. M. Yaghi, *Science*, 2013, **341**, 1230444.
27. S. Qiu, M. Xue and G. Zhu, *Chem. Soc. Rev.*, 2014, **43**, 6116-6140.
28. Z. Kang, L. Fan and D. Sun, *J. Mater. Chem. A*, 2017, DOI: 10.1039/c7ta01142c.
29. F. Zhang, X. Zou, X. Gao, S. Fan, F. Sun, H. Ren and G. Zhu, *Adv. Funct. Mater.*, 2012, **22**, 3583-3590.
30. X. Liu, C. Wang, B. Wang and K. Li, *Adv. Funct. Mater.*, 2017, **27**, 1604311.
31. K. Guan, D. Zhao, M. Zhang, J. Shen, G. Zhou, G. Liu and W. Jin, *J. Membr. Sci.*, 2017, **542**, 41-51.
32. W. Li, Y. Zhang, P. Su, Z. Xu, G. Zhang, C. Shen and Q. Meng, *J. Mater. Chem. A*, 2016, **4**, 18747-18752.

View Article Online
DOI: 10.1039/C8QM00351C

33. M. Jia, Y. Feng, S. Liu, J. Qiu and J. Yao, *J. Membr. Sci.*, 2017, **539**, 172-177.
34. J. Wang, Y. Wang, Y. Zhang, A. Uliana, J. Zhu, J. Liu and B. Van der Bruggen, *ACS applied materials & interfaces*, 2016, **8**, 25508-25519.
35. Y. Ying, D. Liu, W. Zhang, J. Ma, H. Huang, Q. Yang and C. Zhong, *ACS applied materials & interfaces*, 2017, **9**, 1710-1718.
36. H. Yang, N. Wang, L. Wang, H.-X. Liu, Q.-F. An and S. Ji, *J. Membr. Sci.*, 2018, **545**, 158-166.
37. H. Yin, A. Khosravi, L. O'Connor, A. Q. Tagaban, L. Wilson, B. Houck, Q. Liu and M. L. Lind, *Industrial & Engineering Chemistry Research*, 2017, **56**, 9167-9176.
38. X.-L. Liu, Y.-S. Li, G.-Q. Zhu, Y.-J. Ban, L.-Y. Xu and W.-S. Yang, *Angewandte Chemie-International Edition*, 2011, **50**, 10636-10639.
39. R. Zhang, S. Ji, N. Wang, L. Wang, G. Zhang and J. R. Li, *Angew. Chem. Int. Ed. Engl.*, 2014, **53**, 9775-9779.
40. X. Liu, H. Jin, Y. Li, H. Bux, Z. Hu, Y. Ban and W. Yang, *J. Membr. Sci.*, 2013, **428**, 498-506.
41. Y. Mao, J. Li, W. Cao, Y. Ying, P. Hu, Y. Liu, L. Sun, H. Wang, C. Jin and X. Peng, *Nat. Commun.*, 2014, **5**, 5532.
42. G. Zhan and H. C. Zeng, *Adv. Funct. Mater.*, 2016, **26**, 3268-3281.
43. K. Shen, L. Zhang, X. Chen, L. Liu, D. Zhang, Y. Han, J. Chen, J. Long, R. Luque, Y. Li and B. Chen, *Science*, 2018, **359**, 206–210.
44. Z. Chen, B. Holmberg, W. Li, X. Wang, W. Deng, R. Munoz and Y. Yan, *Chem. Mater.*, 2006, **18**, 5669-5675.
45. P. R. H. P. Rao and M. Matsukata, *Chem. Commun.*, 1996, 1441-1442.
46. Yuan Peng, Y. Li, Y. Ban, H. Jin, W. Jiao, X. Liu and W. Yang, *Science*, 2014, **346**, 1356-1359.
47. H. Li, Z. Song, X. Zhang, Y. Huang, S. Li, Y. Mao, H. J. Ploehn, Y. Bao and M. Yu, *Science*, 2013, **342**, 95-98.
48. R. Banerjee, A. Phan, B. Wang, C. Knobler, H. Furukawa, M. O'Keeffe and O. M. Yaghi, *Science*, 2008, **319**, 939-943.
49. J. Han, Y. Shen and W. Feng, *Nanoscale*, 2016, **8**, 14139-14145.
50. J. Shen, G. Liu, K. Huang, W. Jin, K. R. Lee and N. Xu, *Angew. Chem. Int. Ed. Engl.*, 2015, **54**, 578-582.
51. Y.Matsuo, Y.Nishino, T.Fukutsuka and Y.Sugie, *carbon*, 2007, **45**, 1384-1390.
52. N. I. Kovtyukhova, T. E. Mallouk, L. Pan and E. C. Dickey, *J. Am. Chem. Soc.*, 2003, **125**, 9761-9769.
53. M. Yoonessi, Y. Shi, D. A. Scheiman, M. Lebron-Colon, D. M. Tigelaar, R. A. Weiss and M. A. Meador, *ACS nano*, 2012, **6**, 7644-7655
54. C. Chi, X. Wang, Y. Peng, Y. Qian, Z. Hu, J. Dong and D. Zhao, *Chem. Mater.*, 2016, **28**, 2921-2927.
55. D. Wang, Z. Wang, L. Wang, L. Hu and J. Jin, *Nanoscale*, 2015, **7**, 17649-17652.
56. A. Huang, Q. Liu, N. Wang, Y. Zhu and J. Caro, *J. Am. Chem. Soc.*, 2014, **136**, 14686-14689.
57. X. Wang, C. Chi, J. Tao, Y. Peng, S. Ying, Y. Qian, J. Dong, Z. Hu, Y. Gu and D. Zhao, *Chem. Commun.*, 2016, **52**, 8087-8090.
58. F. Cacho-Bailo, I. Matito-Martos, J. Perez-Carbajo, M. Etxeberria-Benavides, O. Karvan, V. Sebastian, S. Calero, C. Tellez and J. Coronas, *Chemical science*, 2017, **8**, 325-333.
59. L. M. Robeson, *J. Membr. Sci.*, 2008, **320**, 390-400.
60. S. U. Rege and R. T. Yang, *Chem. Eng. Sci.*, 2001, **56**, 3781–3796.
61. K. Roztocki, M. Lupa, M. Hodorowicz, I. Senkovska, S. Kaskel and D. Matoga, *CrystEngComm*, 2018, DOI: 10.1039/c8ce00269j.
62. X. Wang, V. Schwartz, J. C. Clark, X. Ma, S. H. Overbury, X. Xu and C. Song, *J. Phys. Chem. C,*, 2009, **113**, 7260–7268.
63. G. Xu, J. Yao, K. Wang, L. He, P. A. Webley, C.-s. Chen and H. Wang, *J. Membr. Sci.*, 2011, **385-386**, 187-193.
64. E. Favre, D. Roizard, R. Bounaceur and W. J. Koros, *Ind. Eng. Chem. Res.*, 2009, **48**, 3700–3701.
65. E. Jeon, S.-Y. Moon, J.-S. Bae and J.-W. Park, *Angew. Chem. Int. Ed*, 2016, **128**, 1340 –1345.
66. L. Ding, Y. Wei, L. Li, T. Zhang, H. Wang, J. Xue, L. X. Ding, S. Wang, J. Caro and Y. Gogotsi, *Nat Commun*, 2018, **9**, 155.
67. H. W. Kim, H. W. Yoon, S.-M. Yoon, B. M. Yoo, B. K. Ahn, Y. H. Cho, H. J. Shin, H. Yang, U. Paik, S. Kwon, J.-Y. Choi and H. B. Park, *Sciene*, 2013, **342**, 91-95.
68. J. Wang, S. Wang, Q. Xin and Y. Li, *J. Mater. Chem. A*, 2017, **5**, 6794-6816.
69. M. Galizia, W. S. Chi, Z. P. Smith, T. C. Merkel, R. W. Baker and B. D. Freeman, *Macromolecules*, 2017, **50**, 7809-7843.
70. J. Lindmark and J. Hedlund, *J. Mater. Chem.*, 2010, **20**, 2219-2225.
71. H. Huang, W. Zhang, D. Liu and C. Zhong, *Industrial & Engineering Chemistry Research*, 2012, **51**, 10031-10038.
72. M. Pourafshari Chenar, M. Soltanieh, T. Matsuura, A. Tabe-Mohammadi and K. C. Khulbe, *J. Membr. Sci.*, 2006, **285**, 265-271.